arXiv:astro-ph/0202417v1 22 Feb 2002

MHD Shock Conditions for Accreting Plasma onto Kerr Black Holes - I

Masaaki Takahashi

Department of Physics and Astronomy, Aichi University of Education, Kariya, Aichi 448-8542, Japan; takahasi@phyas.aichi-edu.ac.jp

and

Darrell Rilett, Keigo Fukumura, and Sachiko Tsuruta

Department of Physics, Montana State University, Bozeman, MT 59717-3840; rilett@physics.montana.edu, fukumura@physics.montana.edu, tsuruta@physics.montana.edu

ABSTRACT

We extend the work by Appl and Camenzind (1988) for special relativistic magnetohydrodynamic (MHD) jets, to fully general relativistic studies of the standing shock formation for accreting MHD plasma in a rotating, stationary and axisymmetric black hole magnetosphere. All the postshock physical quantities are expressed in terms of the relativistic compression ratio, which can be obtained in terms of preshock quantities. Then, the downstream state of a shocked plasma is determined by the upstream state of the accreting plasma. In this paper sample solutions are presented for slow magnetosonic shocks for accreting flows in the equatorial plane. We find that some properties of the slow magnetosonic shock for the rotating magnetosphere can behave like a fast magnetosonic shock. In fact, it is confirmed that in the limit of weak gravity for the upstream non-rotating accretion plasma where the magnetic field lines are leading and rotating, our results are very similar to the fast magnetosonic shock solution by Appl and Camenzind (1988). However, we find that the situation becomes far more complicated due to the effects of strong gravity and rotation, such as the frame dragging-effects. We show the tendency that the large spin of the black hole makes the slow magnetosonic shock strong for the accretion solutions with the same energy-flux.

Subject headings: accretion — black hole physics — MHD — relativity — shock waves

1. Introduction

Recent theoretical and observational developments suggest that various members of active galactic nuclei (AGN) involve supermassive black holes (e.g., Rees (1997)). According to the 'standard unified scenario' an AGN reveals itself as a quasar or a Seyfert nucleus during the earlier stages when the accretion rate is high and the black hole is spinning up, while in later stages when the accretion slows down and the black hole starts losing its rotational energy by spinning down it evolves to a radio galaxy. In the past years physics of black hole magnetospheres has been extensively studied, mainly in connection with winds, jets, and energy extraction from black holes in rotation-powered AGN (Blandford & Znajek (1977); Znajek (1977); Thorne, Price, & Macdonald (1986); see, e.g., Begelman, Blandford & Rees (1984) for comprehensive review). An important step for studying the magnetosphere in the Kerr background space-time was originated by Blandford & Znajek (1977) in the force-free limit. The next logical step will be to extend these magnetospheric studies

to accretion-powered AGN — especially to Seyfert nuclei where the accretion rate should be relatively moderate. Phinney (1983) first extended his general studies of black hole magnetospheres to accretion-powered AGN, adopting the magnetohydrodynamics (MHD). In the early 1990s, Takahashi et al. (1990, hereafter TNTT90), Nitta, Takahashi & Tomimatsu (1991) and Hirotani et al. (1992) investigated both inflow and outflow of material in black hole magnetospheres. Their approach was a general relativistic unified MHD description of both matter accretion process and electromagnetic process in the magnetosphere. Relaxing the force-free limit, these authors explored the roles of interactions between the accreting fluid matter and electromagnetic fields.

Recently, ASCA observations indicated evidence that the Fe lines observed from some Seyfert nuclei are emitted from regions very close to the central black hole (e.g., Tanaka et al. (1995); Nandra et al. (1997)). Iwasawa et al. (1996) interpreted the behavior of Seyfert MCG 6-30-15 deduced from the long ASCA observation as an indication that the black hole is rotating extremely fast, near the maximum limit. Reynolds & Begelman (1997) pointed out that such extremely fast rotation contradicts with the standard unified scenario. Instead, these authors showed that if an X-ray point source somewhere above the hole on the rotation axis illuminates the infalling gas within the inner accretion disk radius, a Schwarzschild hole is consistent with the observation. However, it is not clear how such an X-ray source can be created in the specified location. This issue clearly points to *the importance of investigating, for accretion-powered AGN also, the basic physics of the vicinity very close to a black hole* — especially the regions between the inner boundary of the accretion disk and the event horizon. As our first step toward such investigation, therefore, we explored the standing shock formation in accreting plasmas in black hole magnetospheres. These studies may shed valuable insight to problems such as how X-ray sources can be created near the event horizon.

We consider the central engine of an AGN as a black hole magnetosphere, where magnetized plasma surrounds a black hole and infalling accreting flows and outgoing wind/jets would be generated from the surrounding plasma. We formulate the MHD shock conditions in Kerr geometry for such plasma. The formation of shocks is based on the existence of multi-magnetosonic points in the accretion solution, while for the outgoing plasma the sub-magnetosonic solution is allowable at distant regions. This is because, for instance, the accreting flows initially ejected from a plasma source with low velocity must be terminally super-fast magnetosonic at the event horizon. At the shock front, the flow transits from super-magnetosonic to sub-magnetosonic, so that the accreting flows with a shock must pass through a magnetosonic point on each side of the shock front. This situation is quite similar to the case of hydrodynamical accretion onto a black hole (e.g., Chakrabarti (1990a); Sponholz & Molteni (1994); Lu et al. (1997); Lu & Yuan (1998)). The trans-magnetosonic MHD flow solution was discussed by Takahashi (2000a,b, 2001). Along the magnetic field line, the five physical quantifies are conserved: the total energy E and angular momentum L, the angular frequency of the magnetic field line Ω_F, the particle number flux per magnetic flux tube η, and entropy S (see, e.g., Camenzind (1986a)). When these conserved quantities are specified at the plasma source, the location of the fast/slow magnetosonic points and the Alfvén point are determined. Takahashi (2000a) obtained multi-magnetosonic point solutions and found two regimes of accretion flows – "hydro-like" and "magneto-like". The hydro-like accretion would transit to magneto-like accretion by the shock formation. However, we will postpone, until later, the problem of joining these two types of solutions by shock formation. The reason is that in order to do so we will have to carry out detailed parameter search for trans-magnetosonic MHD flows, but then we will have five field-aligned physical quantities in both upstream and downstream solutions, not a trivial situation. This problem will be additional in a subsequent paper (Rilett et al., in preparation). This paper is meant as a starting point for our long-range investigation of shock conditions for accretion flows in the Kerr geometry. Therefore, here we will only solve the cold trans-fast MHD equations for upstream accretion and discuss the shock properties at the shock fronts. At the

shock front the plasma would be heated up. So, the postshock accretion should be treated by a hot MHD accretion model (Takahashi 2001). In this paper we will not yet solve explicitly the hot trans-magnetosonic solutions for postshock accretion but instead treat the shock front location as a free parameter. However, by joining preshock and postshock solutions, the shock location would be determined at one (or more) place(s).

The main purpose of this paper is to explore the effects of rotation and general relativity on the MHD shock conditions for accreting plasma in a black hole magnetosphere. In order to do so, first in Section 2 we present the basic equations for MHD accretion in the Kerr geometry. Then, in Section 3 we extend the work for special relativistic MHD jets by Appl & Camenzind (1988, hereafter AC88), by deriving the shock conditions for general relativistic MHD accretion onto a Kerr black hole. (Non-relativistic MHD outflow solutions with standing shocks were discussed by Chakrabarti (1990b).) Following AC88, all of our postshock physical quantities are expressed in terms of the relativistic compression ratio ξ. This compression ratio is the solution of a polynomial of eighth degree. Due to the additional factors, namely magnetosphere rotation and general relativistic effects, the mechanism of solution is far more complicated and tedious than in AC88. Our equations reduce to the AC88 equations in the weak gravity limit without plasma rotation. TNTT90 extensively studied MHD accretion flows in the Kerr geometry. As the next step our shock conditions are applied to the accreting MHD plasma flows as described by TNTT90. In Section 4 we present some examples of representative physically relevant shock solutions found for acceptable accretion flows onto the event horizon. Our results are presented for the equatorial flows and slow magnetosonic shocks. The "switch-off" shock (switching-off of the magnetic field at the shock front) and comparison between AC88 and our results are also discussed. More thorough presentation of the results and extensive discussion of the physical implication of these results will be given in Paper II (Rilett et al., in preparation). The general cases including the fast magnetosonic shocks will be presented in Paper III (Rilett et al., in preparation). The possible application of our current work to some astrophysical problems, such as the Seyfert Fe lines, will be given in subsequent papers. Summary and conclusion are given in the last section 5.

2. Basic Equations of General Relativistic Plasma Flow

In this section we summarize the general relativistic MHD flows (see, e.g., Camenzind (1986b, 1989); TNTT90). We assume a stationary and axisymmetric magnetosphere and ignore its self-gravity. We also require infinite conductivity for the plasma flow. The background metric is given by the Boyer-Lindquist coordinates with the $c = G = 1$ units

$$\begin{aligned} ds^2 &= \left(1 - \frac{2mr}{\Sigma}\right) dt^2 + \frac{4amr\sin^2\theta}{\Sigma}\, dt d\phi \\ &\quad - \frac{A\sin^2\theta}{\Sigma}\, d\phi^2 - \frac{\Sigma}{\Delta}\, dr^2 - \Sigma\, d\theta^2 \ , \end{aligned} \tag{1}$$

where $\Delta \equiv r^2 - 2mr + a^2$, $\Sigma \equiv r^2 + a^2\cos^2\theta$, $A \equiv (r^2 + a^2)^2 - a^2\Delta\sin^2\theta$ and m and a denote the mass and angular momentum per unit mass of the black hole, respectively. The basic equations of relativistic plasma flows are as follows: (i) the particle number conservation

$$(nu^\alpha)_{;\alpha} = 0 \ , \tag{2}$$

where n is the proper particle number density and u^α is the fluid 4-velocity; (ii) the conservation of total energy and momentum

$$T^{\alpha\beta}_{\ ;\beta} = 0 \ , \tag{3}$$

where the energy-momentum tensor is given by

$$T^{\alpha\beta} = n\mu u^\alpha u^\beta - Pg^{\alpha\beta} + \frac{1}{4\pi}\left(F^\alpha_{\ \lambda}F^{\lambda\beta} + \frac{1}{4}g^{\alpha\beta}F^2\right) \ , \tag{4}$$

μ is the relativistic specific enthalpy, P is the pressure, $F^{\alpha\beta}$ is the electromagnetic field tensor and $F^2 = F^{\alpha\beta}F_{\alpha\beta}$; and (iii) the MHD condition

$$u^\beta F_{\alpha\beta} = 0 \ . \tag{5}$$

The magnetic field and electric field seen by a distant observer are defined as

$$B_\alpha \equiv \frac{1}{2}\eta_{\alpha\beta\gamma\delta}k^\beta F^{\gamma\delta} \ , \tag{6}$$

$$E_\alpha \equiv F_{\alpha\beta}k^\beta \ , \tag{7}$$

where $k^\alpha = (1,0,0,0)$ is the time-like killing vector and $\eta_{\alpha\beta\gamma\delta} \equiv \sqrt{-g}\,\epsilon_{\alpha\beta\gamma\delta}$. Here, we can introduce the angular velocity of the magnetosphere (see, Bekenstein & Oron (1978))

$$\Omega_F \equiv -\frac{F_{tr}}{F_{\phi r}} = -\frac{F_{t\theta}}{F_{\phi\theta}} \ , \tag{8}$$

which is conserved along magnetic field lines. Then, we obtain the following useful expressions

$$E_\theta = -\sqrt{-g}\,\Omega_F B^r/G_t \ , \tag{9}$$

$$E_r = \sqrt{-g}\,\Omega_F B^\theta/G_t \ , \tag{10}$$

where $G_t \equiv g_{tt} + g_{t\phi}\Omega_F$.

From the conservation of total energy and momentum (3) and the Killing equation $\chi_{\mu;\nu} + \chi_{\nu;\mu} = 0$, where χ^μ is a Killing vector, it follows that $(\chi_\mu T^{\mu\nu})_{;\nu} = 0$ (see, Blandford & Znajek (1977)). Thus, for any stationary and axisymmetric system, we define the conserved energy flux

$$\mathcal{E}^\mu = T^{\mu\nu}k_\nu = T^\mu_t = (T^\mu_t)_{\rm em} + (T^\mu_t)_{\rm fluid} \tag{11}$$

and angular momentum flux

$$-\mathcal{L}^\mu = T^{\mu\nu}m_\nu = T^\mu_\phi = (T^\mu_\phi)_{\rm em} + (T^\mu_\phi)_{\rm fluid} \ , \tag{12}$$

where m^ν is the axial Killing vector with Boyer-Lindquist component (0,0,0,1), and the electromagnetic part and fluid part are labeled by "em" and "fluid", respectively. The fluid and electromagnetic parts of the radial component of energy flux $\mathcal{E}^r$ are

$$\mathcal{E}^r_{\rm fluid} \equiv (T^r_t)_{\rm fluid} = n\mu u^r u_t \ , \tag{13}$$

$$\mathcal{E}^r_{\rm em} \equiv (T^r_t)_{\rm em} = -\frac{B_\phi E_\theta}{4\pi\sqrt{-g}} = \frac{B_\phi B^r \Omega_F}{4\pi G_t} \ , \tag{14}$$

and the fluid and electromagnetic parts of the radial component of angular momentum flux $\mathcal{L}^r$ are

$$-\mathcal{L}^r_{\rm fluid} \equiv (T^r_\phi)_{\rm fluid} = n\mu u^r u_\phi \ , \tag{15}$$

$$-\mathcal{L}^r_{\rm em} \equiv (T^r_\phi)_{\rm em} = -\frac{B_\phi}{4\pi g_{tt}}\left(\frac{g_{t\phi}E_\theta}{\sqrt{-g}} + B^r\right) = -\frac{B_\phi B^r}{4\pi G_t} \ , \tag{16}$$

where we have used the relation (9).

We can express the radial energy and angular momentum fluxes as $\mathcal{E}^r = nu^r E$ and $\mathcal{L}^r = nu^r L$, respectively, where E and L are the total energy and the total angular momentum of the MHD flow seen by a distant observer and defined by

$$E \equiv \mu u_t - \frac{\Omega_F B_\phi}{4\pi\eta} , \tag{17}$$

$$L \equiv -\mu u_\phi - \frac{B_\phi}{4\pi\eta} , \tag{18}$$

and η is the particle number flux per magnetic flux tube defined by

$$\eta \equiv -\frac{nu^r}{B^r} G_t . \tag{19}$$

These quantities E, L and η are conserved along stream lines, which coincide with magnetic field lines (see, Camenzind (1986a)).

The energy and angular momentum of the fluid are

$$\mu u_t = \frac{M^2 E - eG_t}{M^2 - \alpha} , \tag{20}$$

$$\mu u_\phi = -\frac{M^2 L + eG_\phi}{M^2 - \alpha} , \tag{21}$$

where $M^2 \equiv 4\pi\eta^2(\mu/n)$ is the Alfvén Mach number, $e \equiv E - \Omega_F L$, $G_\phi \equiv g_{t\phi} + g_{\phi\phi}\Omega_F$ and $\alpha \equiv G_t + G_\phi \Omega_F$.

The poloidal equation (the relativistic Bernoulli equation) of the magnetized flow is written as

$$(1 + u_p^2) = (E/\mu)^2[(\alpha - 2M^2)f^2 - k] , \tag{22}$$

where

$$f \equiv -\frac{G_\phi + G_t \tilde{L}}{\rho_w (M^2 - \alpha)} , \tag{23}$$

$$k \equiv -(g^{tt} - 2g^{t\phi}\tilde{L} + g^{\phi\phi}\tilde{L}^2) , \tag{24}$$

u_p is the poloidal velocity defined by $u_p^2 \equiv -u^A u_A$ $(A = r, \theta)$, $\rho_w^2 \equiv g_{t\phi}^2 - g_{tt} g_{\phi\phi} = \Delta \sin^2\theta$ and $\tilde{L} \equiv L/E$. We set $u_p > 0$ $(u^r < 0)$ for ingoing flows. When we neglect dissipative effects and cooling in the plasma, the flow is adiabatic with a specific enthalpy of the form (see, Camenzind (1987))

$$\mu = m_{\rm p} + \frac{\Gamma}{\Gamma - 1}\frac{P}{n} , \tag{25}$$

where $m_{\rm p}$ is the rest mass of the particle. The toroidal component of the magnetic field can be expressed as

$$B_\phi = 4\pi\eta \frac{G_\phi E + G_t L}{M^2 - \alpha} . \tag{26}$$

Figure 1 illustrates solutions for the poloidal flow equation (22) for a radial field geometry in the equatorial plane, where the plasma is cold ($P = 0$) with given parameters E, L and Ω_F in the Schwarzschild spacetime. [Note that to determine the magnetic field configuration we should treat the equation of cross-field momentum balance (Grad-Shafranov equation); the general relativistic extension was obtained by Nitta,

Takahashi & Tomimatsu (1991). However, the task is very complicated, so that here we only use a given magnetic field configuration (see section 5).] The flow must pass through the fast magnetosonic point (TNTT90). That is possible only if there is some specific relation $\eta = \eta(E, L, \Omega_F)$; Only for the heavy solid curve with the arrow is this relation satisfied. The physical accretion solution starts from $r = r_{\rm inj}$ with zero poloidal velocity and reaches the event horizon $r = r_{\rm H}$ with a non-zero poloidal velocity. A slow magnetosonic shock should be located between the plasma injection radius $r = r_{\rm inj}$ and the Alfvén radius $r = r_{\rm A}$, if the shock conditions are satisfied. After the slow magnetosonic shock, the heated postshock flow falls into the black hole after passing the slow magnetosonic point, the Alfvén point and the fast magnetosonic point, in this order. The radius of the light surface $r = r_{\rm L}$ and the Alfvén radius $r = r_{\rm A}$ do not change after the shock formation (see the next section).

3. MHD Shocks in Kerr geometry

In order to explore the properties of MHD shocks associated with accretion flows near a black hole, we derive in this section the general relativistic version of MHD shock conditions — an extension of the work by AC88. Figure 2 shows a schematic picture of general accretion inflow from a plasma source, through a shock front, and onto a black hole. In this picture, the accretion originates from the plasma source (which can be the surface of a torus) rotating around a black hole. Strong shocks may be produced somewhere between the plasma source and the event horizon.

3.1. The Jump Conditions

In a complete solution of the accretion that includes a shock, the flow must satisfy a set of conditions on either side of the discontinuity. The jump conditions for arbitrary shocks in a relativistic MHD flow are (e.g., AC88):

$$[nu^\alpha]n_\alpha = 0\ , \quad \text{— the particle number conservation} \tag{27}$$

$$[T^{\alpha\beta}]n_\alpha = 0\ , \quad \text{— the energy momentum conservation} \tag{28}$$

$$[\mathrm{E}] \times \mathrm{n} = 0\ , \quad \text{— the continuity relations for the electric field} \tag{29}$$

$$[\mathrm{B}] \cdot \mathrm{n} = 0\ , \quad \text{— the continuity relations for the magnetic field} \tag{30}$$

where $n^\alpha = (n_0, \mathrm{n})$ and the square brackets denote the difference between the values of a quantity on the two sides of the shock.

We assume that the downstream flow velocity is radial (normal to the event horizon) and the shock front is perpendicular to the downstream flow n=(1,0,0) as shown in Figure 2. Then, we set

$$u_1^\alpha = (u_1^t, u_1^r, u_1^\theta, u_1^\phi)\ , \tag{31}$$

$$u_2^\alpha = (u_2^t, u_2^r, 0, u_2^\phi)\ , \tag{32}$$

$$B_1^\alpha = (B^r, B_1^\theta, B_1^\phi)\ , \tag{33}$$

$$B_2^\alpha = (B^r, 0, B_2^\phi)\ , \tag{34}$$

$$E_1^\alpha = (E_1^r, E^\theta, 0)\ , \tag{35}$$

$$E_2^\alpha = (0, E^\theta, 0)\ , \tag{36}$$

where equations (29) and (30) have been used. The subscripts "1" and "2" denote the preshock and the postshock quantities, respectively. From equation (9), we see that Ω_F does not change across the shock. Equations (27) and (28) evaluated in the shock rest frame yield the following relations

$$n_1 u_1^r = n_2 u_2^r \ , \tag{37}$$

$$\begin{aligned} & n_1\mu_1(u^r u_r)_1 - P_1 + \frac{1}{8\pi g_{tt}}(-E_1^r E_{r1} + B_1^\theta B_{\theta 1} + B_1^\phi B_{\phi 1}) \\ = \ & n_2\mu_2(u^r u_r)_2 - P_2 + \frac{1}{8\pi g_{tt}}(B_2^\phi B_{\phi 2}) \ , \end{aligned} \tag{38}$$

$$n_1\mu_1 u_1^r u_1^\theta - \frac{1}{4\pi g_{tt}}\left(B^r B_1^\theta + E_1^r E^\theta\right) = 0 \ , \tag{39}$$

$$n_1\mu_1 u_1^r u_1^\phi - \frac{B_1^\phi B^r}{4\pi g_{tt}} = n_2\mu_2 u_2^r u_2^\phi - \frac{B_2^\phi B^r}{4\pi g_{tt}} \ , \tag{40}$$

$$n_1\mu_1 u_1^r u_1^t - \frac{1}{4\pi g_{tt}}\left(\frac{B_{\phi 1}E_\theta}{\sqrt{-g}} + B_1^t B^r\right) = n_2\mu_2 u_2^r u_2^t - \frac{1}{4\pi g_{tt}}\left(\frac{B_{\phi 2}E_\theta}{\sqrt{-g}} + B_2^t B^r\right) \ . \tag{41}$$

From the MHD conditions, we also obtain

$$E_{r1}u_{t1} + \sqrt{-g}(B_1^\phi u_1^\theta - B_1^\theta u_1^\phi) = 0 \ , \tag{42}$$

$$(B^r u_1^\phi - B_1^\phi u_1^r)\frac{1}{u_{t1}} = \frac{-E_\theta}{\sqrt{-g}} = (B^r u_2^\phi - B_2^\phi u_2^r)\frac{1}{u_{t2}} \ , \tag{43}$$

$$(g_{t\phi}E_\theta + \sqrt{-g}B^r)u_1^\theta + (g_{t\phi}E_{r1} - \sqrt{-g}B_1^\theta)u_1^r = 0 \ , \tag{44}$$

$$E_{r1}u_1^r + E_{\theta 1}u_1^\theta = 0 \ . \tag{45}$$

From the shock condition of $(T^{rt})_1 = (T^{rt})_2$, we obtain

$$(E - \omega L)_1 = (E - \omega L)_2 \quad , \tag{46}$$

where $\omega \equiv -g_{t\phi}/g_{\phi\phi}$ is the angular velocity of the zero angular momentum observer (ZAMO) with respect to a distant observer, and from the shock condition of $(T^{r\phi})_1 = (T^{r\phi})_2$, we also obtain

$$(g_{t\phi}E + g_{tt}L)_1 = (g_{t\phi}E + g_{tt}L)_2 \quad . \tag{47}$$

From these relations, we see that $E_1 = E_2$ and $L_1 = L_2$. Furthermore, from the particle number conservation and the continuity for electric and magnetic fields at the shock front, we also obtain the relations $(\Omega_F)_1 = (\Omega_F)_2$ and $\eta_1 = \eta_2$. Thus, the field-aligned flow parameters E, L, Ω_F and η are conserved across the shock front. This means that the location of the light surface and the Alfvén radius do not change by a shock generation. The locations of light surfaces $r = r_{\rm L}$ are given by $\alpha = 0$ and the Alfvén radius $r = r_{\rm A}$ is given by $\tilde{L} = -(G_\phi/G_t)_{\rm A}$. Because of the entropy generation ($S_2 > S_1$), the fast/slow magnetosonic points appear at different locations in the preshock and postshock flow solutions. The increasing entropy makes the Alfvén wave speed at the Alfvén point $u_{\rm A}$ [$\equiv u_{\rm AW}(r_{\rm A})$] in a postshock solution smaller than that in a preshock solution.

3.2. Dimensionless Parameters and Their Relations

From the energy momentum conservation at the shock front, we have $(T^{rt})_1 = (T^{rt})_2$, where T^{rt} can be reduced to

$$T^{rt} = g^{tt}(\mathcal{E}^r_{\rm fluid} + \mathcal{E}^r_{\rm em}) - g^{t\phi}(\mathcal{L}^r_{\rm fluid} + \mathcal{L}^r_{\rm em}) \tag{48}$$

$$= g^{tt}\left[n\mu u^r u_t(1-\omega\ell) + \frac{B_\phi B^r(\Omega_F - \omega)}{4\pi G_t}\right] , \tag{49}$$

and $\ell \equiv -u_\phi/u_t$ is the specific angular momentum of the plasma. Here, we define dimensionless parameters. First, we define the "magnetization parameter", which denotes the ratio of the Poynting flux to the total mass-energy flux seen by ZAMO,

$$\sigma \equiv \frac{(\mathcal{E}^r - \omega\mathcal{L}^r)_{\rm em}}{(\mathcal{E}^r - \omega\mathcal{L}^r)_{\rm fluid}} , \tag{50}$$

then we can express equation (48) as

$$T^{rt} = g^{tt}(\mathcal{E}^r - \omega\mathcal{L}^r)_{\rm fluid}(1+\sigma) = (nu^r)(\mu u^t)(1+\sigma) . \tag{51}$$

Then, the magnetization parameter can be reduced to

$$\sigma = \frac{B_\phi}{4\pi\eta(\mu u^t)}\frac{G_\phi}{\rho_w^2} . \tag{52}$$

By using (20) and (21), σ is denoted in terms of M^2, E, L and Ω_F, as

$$\sigma = -\frac{(G_\phi E + G_t L)G_\phi}{\rho_w^2 e + (g_{\phi\phi}E + g_{t\phi}L)M^2} = -\frac{e - h\alpha}{e - hM^2} , \tag{53}$$

where $h \equiv g^{tt}(E - \omega L)$. We can also express M^2 in terms of σ, E, L and Ω_F.

Next, we define the following dimensionless parameters

$$q \equiv \frac{B_2^\phi}{B_1^\phi} = \frac{M_1^2 - \alpha}{M_2^2 - \alpha} , \tag{54}$$

$$\zeta \equiv \frac{\mu_2 u_2^t}{\mu_1 u_1^t} = \frac{e - hM_2^2}{e - hM_1^2} q , \tag{55}$$

$$\xi \equiv \frac{n_2 u_2^t}{n_1 u_1^t} = \frac{M_1^2}{M_2^2}\zeta , \tag{56}$$

where q is the amplification factor for the toroidal magnetic field and ξ is the shock frame compression ratio. From equations (37), (41), (43) we obtain the following relation

$$1 - \zeta = \sigma_1 (q - 1) . \tag{57}$$

The normalization of the 4-velocity gives an equation for u_2^t

$$u_2^t = \left[g_{tt} + 2g_{t\phi}\Omega_2 + g_{\phi\phi}\Omega_2^2 + \frac{(u^r u_r)_1}{\xi^2 (u_1^t)^2}\right]^{-1/2} , \tag{58}$$

where $\Omega \equiv u^\phi/u^t$ is the angular velocity of the fluid, and

$$\Omega_2 = \frac{e\Omega_F - \rho_w^{-2}(g_{t\phi}E + g_{tt}L)M_2^2}{e - hM_2^2} . \tag{59}$$

When other postshock quantities ξ or M_2^2 are determined, u_2^t and Ω_2 can be obtained.

From equation (38), we obtain

$$1-\frac{\zeta}{\xi}-\frac{P_1-P_2}{n_1\mu_1(u^ru_r)_1}+\frac{(-E^rE_r+B^\theta B_\theta+B^\phi B_\phi)_1-(B^\phi B_\phi)_2}{8\pi g_{tt}n_1\mu_1(u^ru_r)_1}=0\ . \tag{60}$$

Using the relations

$$-E^rE_r+B^\theta B_\theta = \frac{g_{tt}\alpha}{G_t^2}B^\theta B_\theta\ , \tag{61}$$

$$(B^\phi B_\phi)_1-(B^\phi B_\phi)_2 = (B^\phi B_\phi)_1(1-q^2)\ , \tag{62}$$

we get

$$1-\frac{\zeta}{\xi}=\Pi-\mathcal{X}_1+(q^2-1)\mathcal{T}_1 \tag{63}$$

with

$$\Pi \equiv \frac{P_1-P_2}{n_1\mu_1(u^ru_r)_1} = 1-\frac{1}{\xi}+\frac{\sigma_1}{\xi}(q-1)+\mathcal{X}_1-(q^2-1)\mathcal{T}_1\ , \tag{64}$$

$$\mathcal{X}_1 \equiv \frac{\alpha(B^\theta B_\theta)_1}{2B^rB_rM_1^2}\ , \tag{65}$$

$$\mathcal{T}_1 \equiv \frac{\sigma_1}{2}\left(\frac{u_t}{u^r}\right)_1^2\frac{\rho_w^2(\Omega_1-\Omega_F)}{g_{rr}G_\phi}\ , \tag{66}$$

which depend on ξ, q and upstream parameters M_1^2 (or σ_1), E, L and Ω_F. The relation between M_2^2 and M_1^2 are given by the poloidal equation (22). (At the shock location $r=r_{\rm sh}$, both $M^2=M_1^2$ and $M^2=M_2^2$ are solutions of the poloidal equation.)

In the following, for preshock accretion flows we restrict ourselves to the cold limit ($P_1=0$). Using the definition of ζ and the equation of state for a Boltzmann gas with the polytropic index Γ

$$\mu_1 = m_{\rm p} \tag{67}$$

$$\mu_2 = m_{\rm p}\left(1+\frac{\Gamma}{\Gamma-1}\frac{P_2}{n_2m_{\rm p}}\right)\ , \tag{68}$$

we find with equation (64)

$$1-\frac{u_2^t}{u_1^t}=\sigma_1(q-1)-\frac{\Gamma}{\Gamma-1}\frac{g_{rr}(u^r/u^t)_1^2(u_2^t)^2}{\xi}\Pi\ . \tag{69}$$

Combining equations (54), (56) and (57) gives the quadratic equation for ζ

$$\zeta^2-\left[1+\sigma_1+\left(\frac{G_t}{M_1^2}-\frac{\sigma_1\Omega_F}{\Omega_F-\Omega_1}\right)\xi\right]\zeta+\left(\frac{G_t}{M_1^2}-\frac{\sigma_1\Omega_1}{\Omega_F-\Omega_1}\right)\xi=0\ , \tag{70}$$

where we use the relation $\Omega-\Omega_F=\sigma M^2/G_\phi$. We are now able to eliminate u_2^t and q from equation (69). After considerable manipulations we obtained a polynomial of eighth degree in ξ

$$\sum_{i=0}^{8}c_i(M_1^2,\Gamma;m,a,E,L,\Omega_F,\eta)\xi^i=0\ . \tag{71}$$

The coefficients c_i are dependent only on upstream parameters, except for Γ which is a function of the downstream temperature involving the modified Bessel functions (Synge 1957)

$$\Gamma(\Theta) = 1 + \left[\frac{1}{\Theta}\left(\frac{K_1(1/\Theta)}{K_2(1/\Theta)} - 1\right) + 3\right]^{-1} \tag{72}$$

with $\Theta = kT/m_{\rm p}$. Θ is related to ξ though

$$\Theta = -g_{rr}u_1^t u_2^t (u_1^r/u_1^t)^2 \Pi/\xi \ . \tag{73}$$

Thus, the compression ratio ξ is the solution of a polynomial (71), which has to be solved simultaneously with equation (72) for the polytropic index Γ for the shocked plasma. The concrete expressions of the coefficients c_i are quite lengthly, so that we only show numerical results in the next section. This polynomial of eighth degree has in general several real solutions corresponding to the different shock transitions. The downstream quantities ζ, q, u_2^t, u_2^r, Ω_2 and Π are also obtained from equations (70), (54), (58), (37), (59) and (64), respectively.

4. Results and Discussions for Slow Magnetosonic Shocks

To see the general shock behavior which depends on flow parameters with the hole's spin a, we present solutions to the coupled equations (71) and (72) for a range of black hole spins. For computational reasons, instead of equation (72) we use a polynomial approximation given by Service (1986). In this paper, we restrict ourselves to slow magnetosonic shocks, which should be located between the plasma source and the Alfvén point. Then, we will only treat the sub-Alfvénic region of $M < M_{\rm A}$ on a trans-fast MHD accretion solution, which is considered as a preshock accretion solution and is assumed cold. This preshock accretion is super-slow magnetosonic. The postshock accretion would be heated up at the shock front, and the slow magnetosonic wave in the hot plasma has a non-zero wave speed $(u_{\rm SM})_2 > 0$, where $u_{\rm SM}$ is the slow magnetosonic wave speed (see, TNTT90). Then, the hot postshock accretion must satisfy the condition $0 < u_{p2} < (u_{\rm SM})_2$ at the shock location; that is, the postshock flow must be sub-slow magnetosonic. All our preshock accretion solutions presented in this paper refer to physically acceptable accretion flows, in the sense that the critical condition (as shown as an example in Fig. 1) is satisfied.

Since we have four conserved parameters, E, L, Ω_F and η, two of these quantities are kept the same for all spin parameters. (The physical descriptions of the parameters are summarized in Table 1.) Fixing L and Ω_F would prevent the formation of shocks across the entire spin range, and so E and η were held constant. Then, physical parameter sets for the trans-fast MHD accretion solutions are calculated. The trans-fast MHD accretion solutions were then obtained by letting Ω_F increase and L (and thus e) decrease linearly with increasing spin a (Table 2). For simplicity, we set the flow to be in the equatorial plane of the radial field geometry $B^r = B_{\rm inj}G_t/\Sigma$ and $B^\theta = 0$ (and then $u^\theta = 0$). $B_{\rm inj}$ is the strength of the field at the plasma injection point. Here, we should note that the radii of $r = r_{\rm H} \equiv m + \sqrt{m^2 - a^2}$, $r = r_{\rm F}$, $r = r_{\rm L}$, $r = r_{\rm A}$ and $r = r_{\rm inj}$ are different for each flow solutions. For larger spin a, the region of $r_{\rm A} < r < r_{\rm inj}$, where the slow magnetosonic shock is expected, becomes narrow and shifts inward (toward the horizon).

In figures 3 and 4 we show the effect of black hole rotation on the nature of shock and accretion flows. The spin parameters selected are $a/m = 0.95$, 0.3, 0.0, -0.2 and -0.4. (In this paper we only calculate the cases $\Omega_F > \omega_{\rm H}$.) In the figures the solid curves are for the maximum a ($= 0.95m$), and the spin decreases as it changes from the solid to the dot-dashed curves which are the minimum at $a = -0.4m$. Positive a refers

to black hole and magnetosphere corotation, while negative a refers to the counter-rotation. No solutions were found for $a < -0.4m$. This is due to the choice of conserved quantities.

Figures 3a, 3b, 3c and 3d show the shock frame compression ratio ξ, thermal pressure Π, polytropic index Γ, and temperature parameter Θ, respectively, as a function of $v_1^{\hat{r}}$, where $v^{\hat{r}} \equiv -(\sqrt{A}/\Delta)u^r/u^t$ is the positive radial 3-velocity of the infalling plasma as seen by a ZAMO. The parameters Π, Γ and Θ refer to the downstream values. Figure 3a shows in general that the compression ratio ξ increases and then decreases with velocity. Figures 3a and 3b show that both ξ and Π increase with increasing black hole rotation. Thermal energy kT (or Θ) and polytropic index Γ for postshock flow have a weak dependence on the black hole spin, but the general trend is that for a given velocity, Γ slightly decreases while Θ slightly increases with increasing $|a|$. Figures 4a, 4b and 4c show the effect of velocity on three other interesting parameters — the ratio of downstream toroidal magnetic field to upstream toroidal magnetic field q, the ratio of downstream number density to upstream number density n_2/n_1, and the upstream magnetization parameter σ_1. We find that q generally decreases while the ratio of the postshock to preshock density increases with the velocity. The effect of larger spin is to enhance the density jump while the azimuthal magnetic field amplification and magnetization are suppressed. In Figure 4a, we can see the switch-off shock, except for the counter-rotating black hole cases. The switch-off shock occurs in the limit when the flow velocity equals the Alfvén wave speed at $r_{\rm sh} = r_{\rm A}$. At this limit, for the postshock flow the toroidal magnetic field B_2^{ϕ} seen by distant observers becomes zero ($q = 0$). When the shock happens close to the Alfvén point, a very hot plasma region is generated (the small spots in Fig. 3d). This region could emit X-rays and γ-rays around the black hole.

In the Newtonian analogy, we expect that for the strong shock $n_2/n_1 \sim 4$ for $\Gamma = 5/3$ and $n_2/n_1 \sim 7$ for $\Gamma = 4/3$. In the Schwarzschild black hole case, for example, we obtain a similar tendency for the maximum values; that is, $n_2/n_1 \sim 4$ for $\Gamma = 5/3$ and $n_2/n_1 \geq 8$ for $\Gamma = 1.4$ (see Figs. 3c and 4b). The compression ratio also has a maximum $\xi_{\rm max} \approx 3.6$ for $a = 0$ and $\xi_{\rm max} \geq 4$ for $a = 0.95m$ (Fig. 3a). Compared with the n_2/n_1 vs $v_1^{\hat{r}}$ diagram, $\xi(v_1^{\hat{r}})$ is almost constant for the strong shocks (i.e., $a > 0$). This is due to the effect of factor u_2^t/u_1^t (see, eq. (56)). From Figures 3a and 4b, it may appear that a strong shock is possible for very low accretion speed (for $a > -0.2m$). Note that in our calculation, we set $\eta =$ constant ($\eta \propto nu^r \neq 0$), so $v_1^{\hat{r}} \ll 1$ means $n_1 \gg 1$. When $v_1^{\hat{r}} \ll 1$, the postshock flow must also satisfy $v_2^{\hat{r}} \ll 1$, and then $n_2 \gg 1$. Thus, as a result of numerical calculation, we obtain a finite value for n_2/n_1 in the limit of $v_1^{\hat{r}} \to 0$.

Figures 5a and 5b show the ξ vs. $v_1^{\hat{\phi}}$ and $v_1^{\hat{\phi}}$ vs. $v_1^{\hat{r}}$ relations, where $v^{\hat{\phi}} \equiv (-g_{\phi\phi}/\rho_w)(\Omega - \omega)$ is the toroidal 3-velocity seen by a ZAMO. Figure 5b shows that when its radial velocity is very low, such a flow does possess sufficiently large toroidal velocity (especially the $a = 0.95m$ case). The negative $v_1^{\hat{\phi}}$ is due to the effect of dragging on the plasma by the counter-rotating black hole. The toroidal velocity $v_1^{\hat{\phi}}$ is explicitly related to the toroidal magnetic field $(B_\phi)_1$, and therefore it can be also related to the magnetization parameter σ_1 (see Fig. 4c). The difference of σ_1 between the corotating black hole case and the counter-rotating black hole case is caused by this spin-dependence of the toroidal motion. That is, due to the dragging effects, $|B_\phi|_1$ is forced to decrease for $a = 0.95m$, while it is forced to increase by stretching toward the $(-\phi)$-direction for the $a = -0.4m$ case. We also obtain the result that $(v_2^{\hat{\phi}} - v_1^{\hat{\phi}}) \to 0$ and the magnetic field line is tangent to the shock surface when $v_1^{\hat{r}} \to 0$. Figure 5c shows the ξ vs. $r_{\rm sh}$ relation. For a magnetosphere with a large spin the shock front is located near the event horizon, and a strong shock is generated. Along each curve the shock strength increases slightly when the shock location shifts inward from the vicinity of the plasma source, but near the Alfvén point it decreases considerably.

We extended the work by AC88 on the MHD shock conditions for special relativistic jets, by deriving corresponding equations for general relativistic accretion flows in the magnetosphere of a rotating black hole.

Our results refer to the slow magnetosonic shock for accretion flows very close to a black hole where the general relativistic effects are strong, while the AC88 results refer to the fast magnetosonic shock for outflows at long distances away from the hole. The one apparent difference between our results and those by AC88 is that their r (our ξ) and $\Pi \to 0$ sharply as their $\beta \to 0$, while our ξ and Π do not drop off sharply as $v_1^{\hat{r}} \to 0$ (see our Figures 3a and 3b). (In the rest of the velocity range, we find that the general trend of our results and theirs is quite similar, especially for positive a.) Another difference is the velocity dependence of q. For the fast magnetosonic shock in the case of AC88, there is a lower-limit threshold for the upstream velocity $v_1^{\hat{r}}$ to satisfy the requirement of $q > 1$. When this lower-limit velocity is approached (where $q = 1$), the compression ratio decreases, and below this velocity there is no fast magnetosonic shock solutions. On the other hand, for the slow magnetosonic shock in our case, the condition $q < 1$ is required, and moreover there is not such a threshold for the lower limit to the upstream velocity and ξ does not drop off. For $v_1^{\hat{r}} \to 0$ we obtain $q = 1$, and for the switch-off shock (if present) we obtain $q = 0$ (see Fig. 4a). The switch-off shock gives the upper limit to the upstream flow velocity, which is just the Alfvén wave velocity. Note that in the rotating black hole case the velocity range that allows to the slow magnetosonic shock is restricted by some other factors — for instance, due to the dragging effect.

The general behavior of Γ and Θ with velocity for all spin parameters a as exhibited in Figures 3c and 3d are essentially the same as Figure 6 of AC88 for hydrodynamic shocks with no plasma rotation. As mentioned by AC88, we also find that the polytropic index for the postshock plasma stays closer to 5/3 than to 4/3, except for extremely high Lorentz factors; here we should note that, for small $v_1^{\hat{r}}$, Γ remains $\sim 5/3$ even when $v_1^{\hat{\phi}}$ dominates the flow velocity.

We note that our equations derived in Section 3.2 reduce to the corresponding equations in AC88 in the limit of no plasma rotation and weak gravity ($\Omega_1 = 0$, $m = 0$ and $a = 0$). With more direct comparison with AC88 in mind, we present in Figure 6 the result for the asymptotic case of $a = 0$, $\Omega_1 = 0$, slowly rotating magnetosphere $\Omega_F \ll 1$, and large distance, closer to the situation investigated by AC88. Figure 6a shows the compression ratio vs. $v_1^{\hat{r}}$ relation, while in Figure 6b the adiabatic exponent and temperature parameter are shown as a function of $v_1^{\hat{r}}$. The chosen conserved quantities are given in Table 3. These parameters appear to put us in the small b' and small θ' regime (small σ) of AC88. Figures 6a and 6b show that although the parameters chosen here and AC88 are somewhat different, these curves are essentially identical to figures 1 and 6 of AC88. (Note that figure 6 in AC88 shows the hydrodynamical shock case.)

Though our results of slow magnetosonic shocks for $a > 0$ are very similar to the AC88 results obtained for the fast magnetosonic shocks, the local physical properties are obviously different between the fast and slow magnetosonic shocks. Here, we should note that our results include the rotational effects of magnetic field lines, which are leading the black hole toward the rotational direction. So this apparent similarity is caused essentially by the rotation of the magnetic field lines. When $0 < \Omega_1 < \Omega_F$, we find that $\Omega_1 < \Omega_2 < \Omega_F$. This means that in our slow magnetosonic shock case the trajectory of a fluid element seen by a distant observer becomes very similar to the fast magnetosonic shock case without rotation, as shown in Figure 7a. On the other hand, in the shock frame rotating with Ω_F, the trajectory of a fluid element in our case is coincident with the magnetic field pattern (see Fig. 7b). So, some shock properties of the slow magnetosonic shock with $\Omega_1 > 0$ behave like the fast magnetosonic shock without rotation (especially the hydrodynamical behavior). This is not essentially due to the general relativistic effects, but the existence of the slowly rotating black hole ($0 < \omega_{\rm H} < \Omega_F$), or a counter-rotating black hole ($\Omega_F \omega_{\rm H} < 0$), is responsible for such a situation (with the magnetic field lines leading the black hole in rotation) in the rotating magnetosphere. When $\Omega_1 < 0$, which state is easily realized for a rapidly counter-rotating black hole, the downstream plasma angular velocity Ω_2 is in the range of $\Omega_1 < \Omega_2 \leq 0$ or $0 < \Omega_2 < \Omega_F$, and the trajectory of the fluid is quite

different from the fast magnetosonic shock case, and then the shock behavior is also different. Also, for a rapidly rotating black hole with $0 < \Omega_F < \omega_{\rm H}$ and the magnetic field lines trailing the black hole in the rotational direction, this similarity would be lost except for the very strong shock cases. Note that the dominant energy dissipation and accompanying radiation processes in the postshock hot plasma would be different between the *corotating* slow magnetosonic shock and the fast magnetosonic shock without rotation, even if some of their properties are very similar.

Finally in Figure 8 we show our preliminary results for the upstream (solid curve) and downstream (dashed curve) magnetization parameters, σ_1 and σ_2, plotted as a function of the shock location, $r_{\rm sh}$, for a representative spin of $a = 0.7m$. The conserved quantities chosen for this spin parameter are given in Table 2. From the energy momentum conservation at the shock front with equation (51), the postshock magnetization parameter σ_2 is expressed as $\sigma_2 = \zeta^{-1}\sigma_1 + (\zeta^{-1} - 1)$. The decreasing σ across the shock means that $\zeta > 1$. Although, at the shock front, kinetic energy of the preshock flow obviously converts to thermal energy of the postshock flow, the electromagnetic energy also converts to thermal energy at the same shock front. At the location of $r_{\rm sh} \to r_{\rm A}$ (when the switch-off shock takes place), the energy conversion is maximum. The detailed transitions of each of the energy components and the discussion of the implications will be presented in Paper II (Rilett et al., in preparation).

5. Summary and Concluding Remarks

The main purpose of this paper is to explore the general relativistic version of MHD shock conditions for accreting plasma in a magnetosphere of a rotating black hole. Here, we introduce the magnetization parameter seen by ZAMO, because the shock conditions are related to the local plasma and the magnetosphere is dragged by the rotating black hole. Then, we can obtain similar expressions as for the special relativistic case, though the formulae include the Kerr metric. We have seen that the compression ratio ξ is the solution of a polynomial of eighth degree.

Although the jump condition is of course determined by the local physics, for a distant observer, the shock properties depend also on the gravitational field structure (i.e., the gravitational redshift factor and the dragging effect, etc); furthermore, the preshock plasma flow parameters are also affected by the gravity and its spin. So, when we observe some physical properties of the magnetosonic shock, which may be related to some efficient radiation process, we should understand the gravitational field structure in addition to the properties of magnetized plasma flow.

In this paper our sample solutions are presented for the special case of slow magnetosonic shocks in plasmas accreting in the equatorial plane with the radial magnetic field configuration. For slow magnetosonic shocks our results are compared with those by AC88. It is confirmed that, though AC88 discussed fast magnetosonic shocks, the general agreement is excellent in the limit of no plasma rotation and weak gravity. However, with the introduction of additional factors, gravity and rotation, we find that the situation becomes far more complicated. For example, in a black hole magnetosphere, two Alfvén points and two slow magnetosonic points can be located inside the separation point $r = r_{\rm sp}$, where the gravitational force and the centrifugal force are balanced for plasma with zero poloidal velocity and the radius is defined by $(\alpha')_{\rm sp} = 0$; the prime means the derivative along a stream line. In this paper we have treated only cold MHD accreting flow passing through the inner Alfvén point. However, the MHD accretion flow passing through the outer Alfvén point is also possible. In both cases the injection point can be located near (inside) the separation point. When we consider shock formation where the postshock flow passes through the outer Alfvén point,

we would find such a flow as an additional branch in the figures such as those presented in this paper. Such a new branch would appear outside the previous branch, and it of course must be located between the outer Alfvén point and the injection point. However, the postshock accretion flow may pass through the inner Alfvén point. Furthermore, to obtain the accretion flow passing through the fast magnetosonic point twice by the shock formation, we must more carefully find the acceptable parameter ranges of conserved quantities. This will be our next step. In non-relativistic flow solutions, Chakrabarti (1990b) discussed the slow and fast magnetosonic point conditions and shock conditions in winds, where multi-magnetosonic wind solutions were demonstrated. In the future, we will extend our results by treating a multi-magnetosonic flow conditions with shock formation in the Kerr geometry.

As a preliminary example of how the transition of various parameters behave across the shock front, in Figure 8 we showed the preshock and postshock magnetization parameters. The detailed results for the transition behavior of various energy components and other parameters will be presented in Paper II (Rilett et al., in preparation). Here we only comment that both fluid kinetic energy and electromagnetic energy convert to thermal energy at the shock location.

When we consider accretion through high-latitude regions above the event horizon near the hole's rotational axis (see Nitta, Takahashi & Tomimatsu (1991); Tomimatsu & Takahashi (2001)), we can expect as an X-ray source hot ringed area around the axis. Our extended future work will include the application of our current work to realistic models of a black hole magnetosphere as the central engine of accretion-powered AGN.

We are grateful to Akira Tomimatsu and Hideyo Kunieda for useful discussions. S.T. thanks the Yamada Foundation for financial support through the visiting program.

REFERENCES

Appl, S., & Camenzind, M. 1988, A&A, 206, 258, AC88

Begelman, M. C., Blandford, R. D., & Rees, M. J. 1984, Rev. Mod. Phys., 56, 255

Bekenstein, J. D., & Oron, E. 1978, Phys. Rev. D, 18, 1809

Blandford, R. D., & Znajek, R. L. 1977, MNRAS, 179, 433

Camenzind, M. 1986a, A&A, 156, 137

Camenzind, M. 1986b, A&A, 162, 32

Camenzind, M. 1987, A&A, 184, 341

Camenzind, M. 1989, *in Accretion Disks and Magnetic Fields in Astrophysics*, ed. G. Belvedere (Dordrecht: Kluwer), P.129

Chakrabarti, S. K. 1990a, ApJ, 350, 275

Chakrabarti, S. K. 1990b MNRAS, 246, 134

Nandra, K., George, I. M., Mushotzky, R. F., Turner, T.J., & Yaqoob, T. 1997, ApJ, 488, 91

Nitta, S., Takahashi, M. & Tomimatsu, A. 1991, Phys. Rev. D, 44, 2295

Hirotani, K., Takahashi, M., Nitta, S., & Tomimatsu, A. 1992, ApJ, 386, 455

Iwasawa, K., et al. 1996, MNRAS, 282, 1038

Lu, J.-F, Yu, K.N., Yuan, F., & Young, E. C. M. 1997, A&A, 321, 665

Lu, J.-F, & Yuan, F. 1998, MNRAS, 295, 66

Phinney, E.S. 1983, Ph.D. thesis, Univ. Cambridge

Rees, M. J. 1997, in Proceedings of S. Chandrasekher Memorial Conference (Chicago: Univ. of Chicago Press), 83

Reynolds, C. S., & Begelman, M. C. 1997, ApJ, 488, 109

Service, A. T. 1986, ApJ, 307, 6

Sponholz, H., & Molteni, D. 1994, MNRAS, 271, 233

Synge, J. L. 1957, The Relativistic Gas (North Holland)

Takahashi, M., Nitta, S., Tatematsu, Y., & Tomimatsu, A. 1990, ApJ, 363, 206, TNTT90

Takahashi, M. 2000a, in Proceedings of the 19th Texas Symposium on Relativistic Astrophysics and Cosmology, ed. E. Aubourg, T. Montmerle, L. Paul & P. Peter (North-Holland, Amsterdam) CD-ROM 01/27.

Takahashi, M. 2000b, Il Nuovo Cimento, 115, 843

Takahashi, M. 2001, ApJ, submitted

Tanaka, Y., et al. 1995, Nature, 375, 659

Thorne, K. S., Price, R. H., & Macdonald, D. A., eds. 1986, Black Hole: The Membrane Paradigm (New Haven: Yale Univ. Press)

Tomimatsu, A. & Takahashi, M. 2001, ApJ, 552, 710

Znajek, R. L. 1977, MNRAS, 179, 457

This preprint was prepared with the AAS LaTeX macros v5.0.

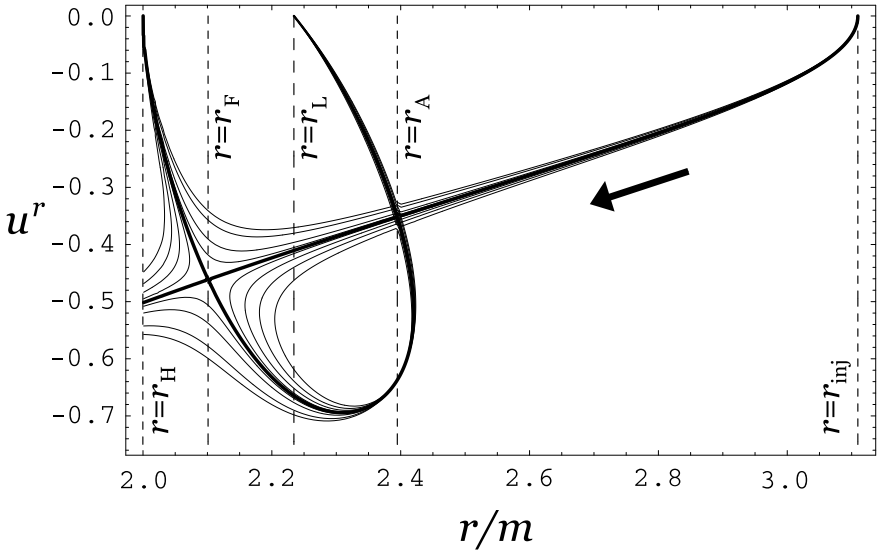

Fig. 1.— A preshock cold trans-fast MHD accretion solution ($\eta = \eta_{\rm F}$; bold curve with arrow). The solution with zero-velocity at the event horizon $r = r_{\rm H}$ is unphysical. The other solutions ($\eta \neq \eta_{\rm F}$; thin curves) are also unphysical. The radii of $r = r_{\rm F}$, $r = r_{\rm L}$, $r = r_{\rm A}$ and $r = r_{\rm inj}$ are the locations of the fast magnetosonic point, the light surface, the Alfvén point and the injection point, respectively. A slow magnetosonic shock would be possible somewhere between the plasma injection radius and the Alfvén radius.

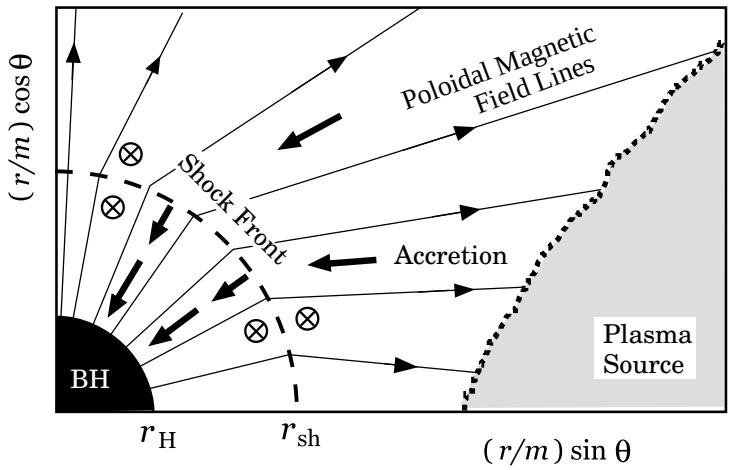

Fig. 2.— Accretion flows with shock front. It is assumed that in the poloidal plane the downstream flow is radial and the shock front distributes perpendicular to the the downstream flow direction. In a general case, the magnetic field has a non-zero toroidal component (marked by $\otimes$) because of the plasma rotation.

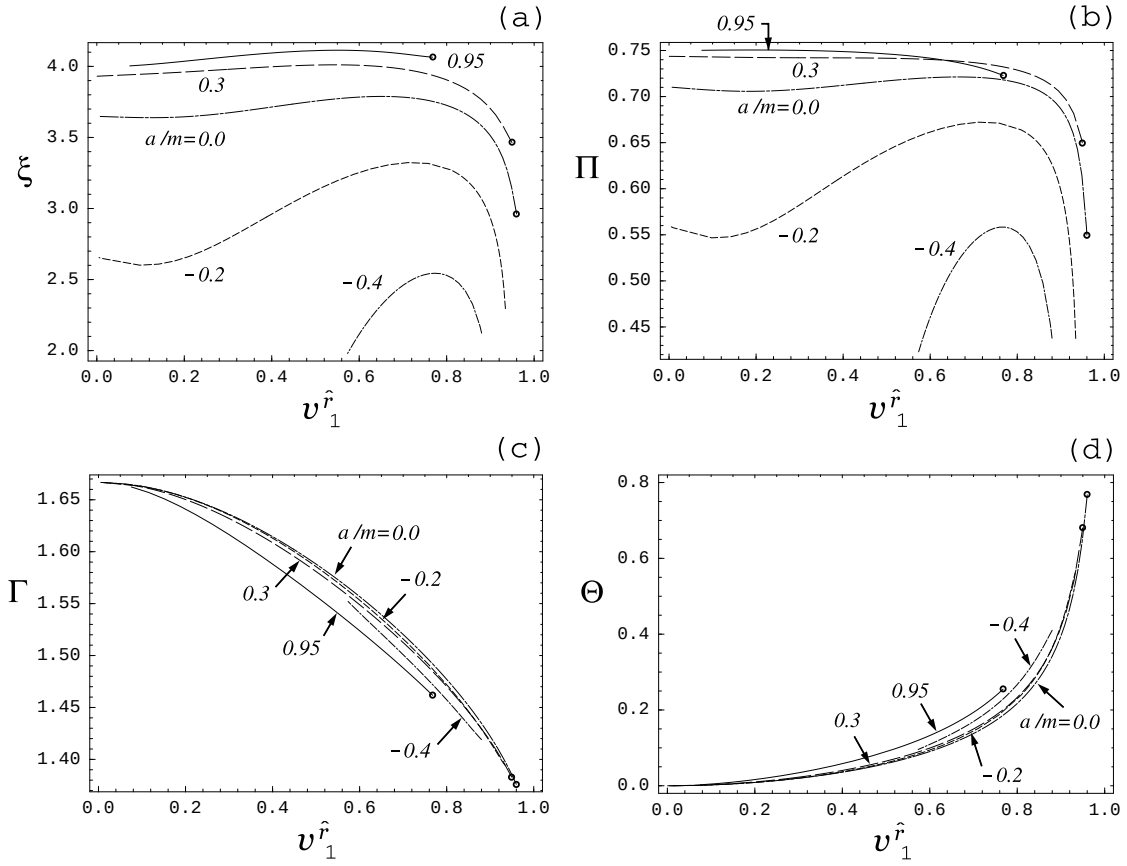

Fig. 3.— (a) The shock frame compression ratio ξ, (b) thermal pressure Π, (c) polytropic index Γ, and (d) temperature parameter Θ, respectively, as a function of $v_1^{\hat{r}}$, the radial velocity of the infalling plasma, for variable spin parameters ($a/m = 0.95, 0.3, 0.0, -0.2, -0.4$). The parameters Π, Γ and Θ refer to the downstream values. The shocks at the switch-off points are shown by small spots. The sets of field aligned parameters are given in Table 2.

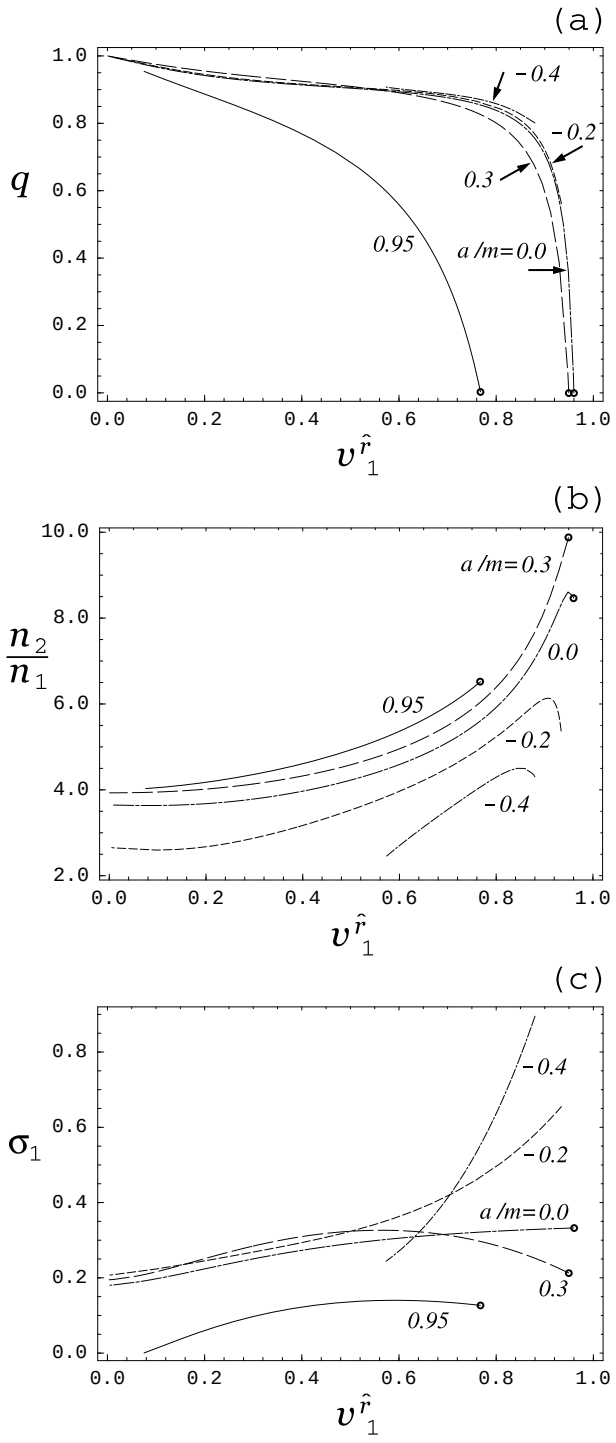

Fig. 4.— Various parameters are shown as a function of $v_1^{\hat{r}}$. (a) The ratio of the downstream toroidal magnetic field to upstream toroidal magnetic field q, (b) the ratio of the downstream number density to upstream number density, and (c) the upstream magnetization parameter σ_1. The chosen parameter sets are the same as in Fig. 3.

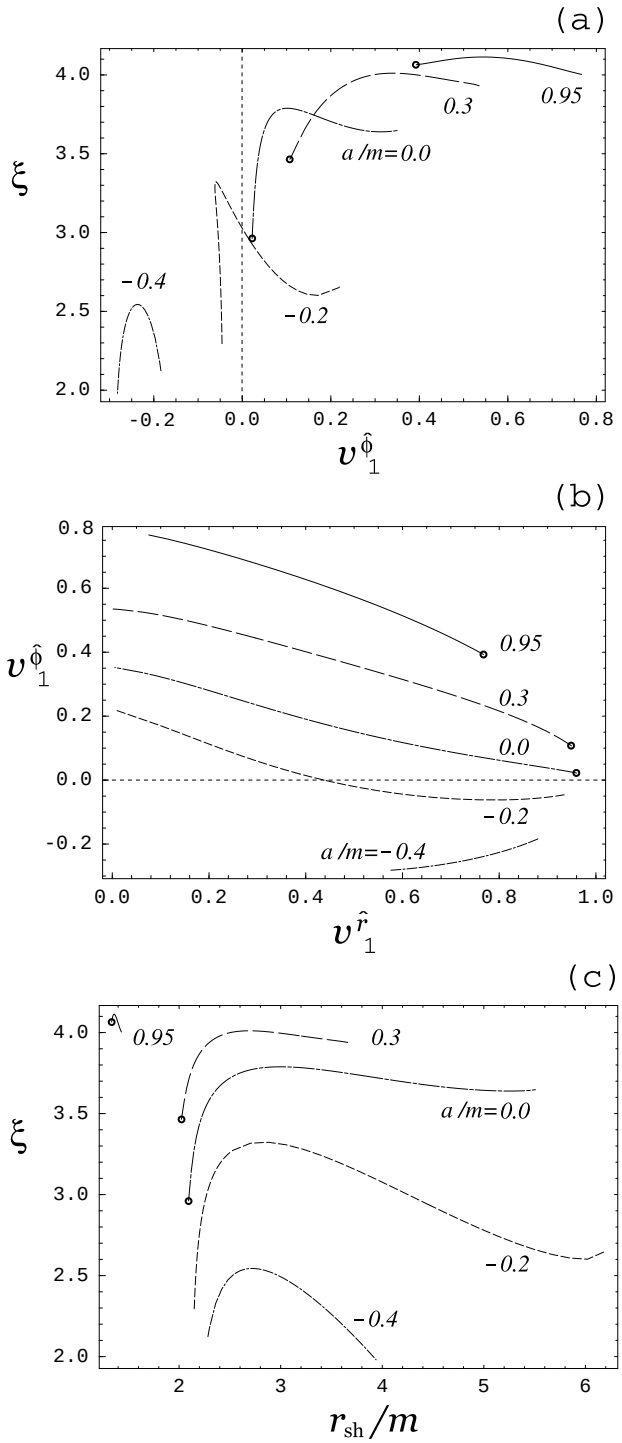

Fig. 5.— (a) The compression ratio as a function of $v_1^{\hat{\phi}}$, (b) the toroidal velocity $v_1^{\hat{\phi}}$ as a function of $v_1^{\hat{r}}$, and (c) the compression ratio ξ as a function of the shock location $r_{\rm sh}$. The parameter sets are the same as in Fig. 3.

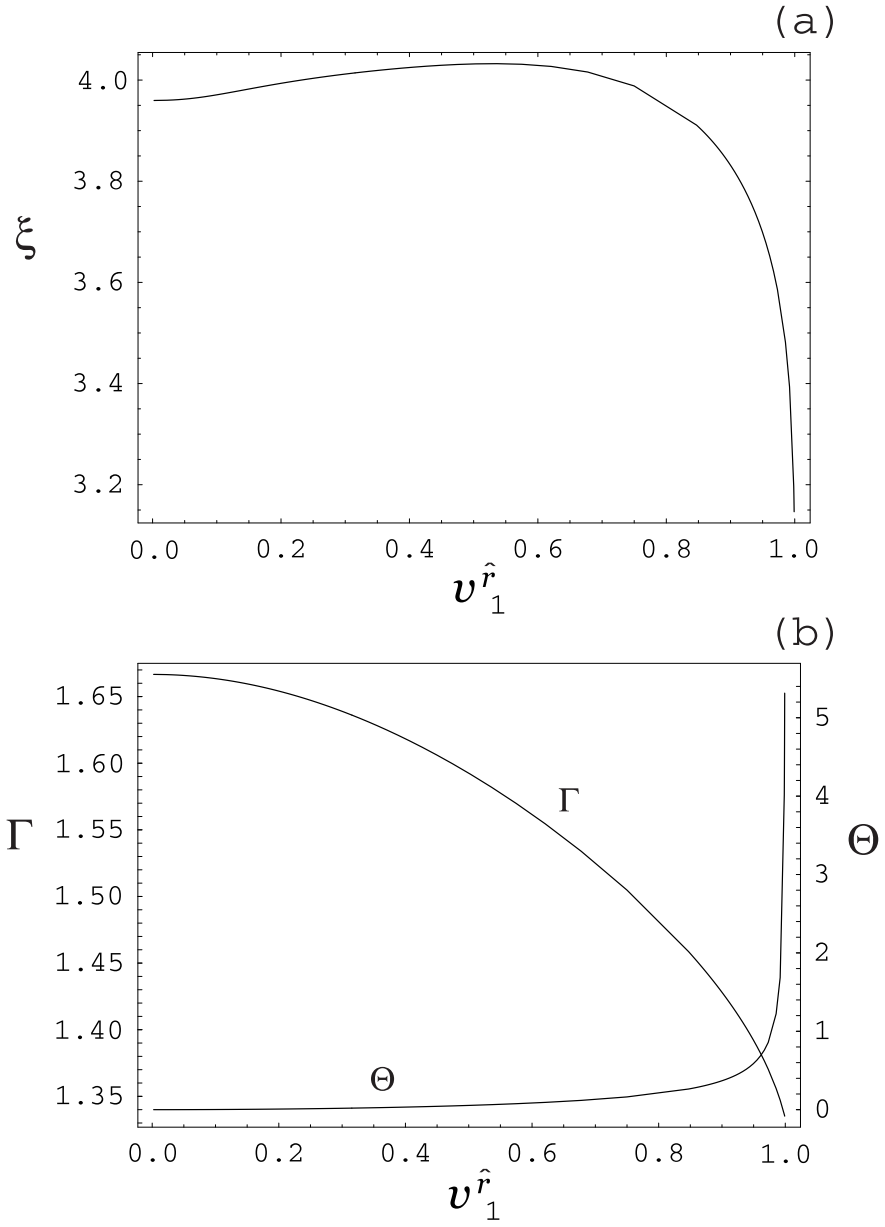

Fig. 6.— (a) The shock frame compression ratio ξ, and (b) polytropic index Γ and temperature parameter Θ, respectively, as a function of the radial preshock velocity $v_1^{\hat{r}}$ in the limit of no plasma rotation and weak gravity ($\Omega_1 = 0$, $m = 0$, $a = 0$). The set of field aligned parameters is given in Table 3.

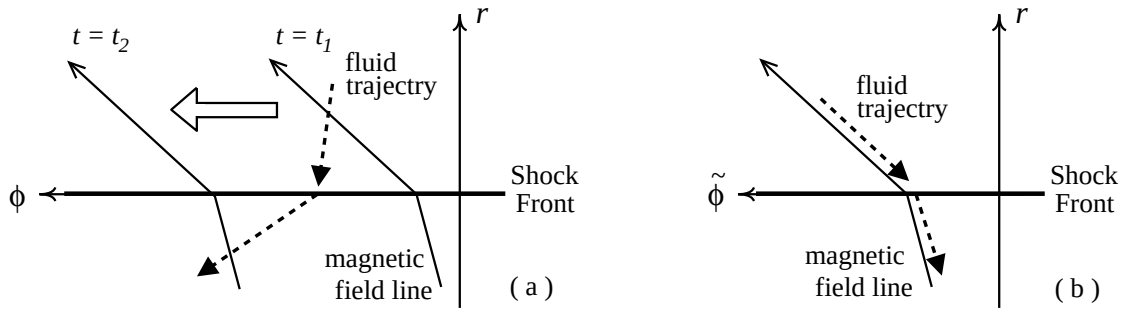

Fig. 7.— The slow magnetosonic shock seen by (a) a distant observer in the (r, ϕ)-plane and (b) a shock frame observer in the $(r, \tilde{\phi})$-plane, which is corotating with the magnetic field line. For a slowly rotating black hole case ($\omega_{\rm H} < \Omega_F$), the magnetic field lines are leading the black hole toward the rotational direction, and the fluid trajectory across the shock front looks like the fast magnetosonic shock case; and then some physical properties of the slow magnetosonic shock is very similar to that of the fast magnetosonic shock.

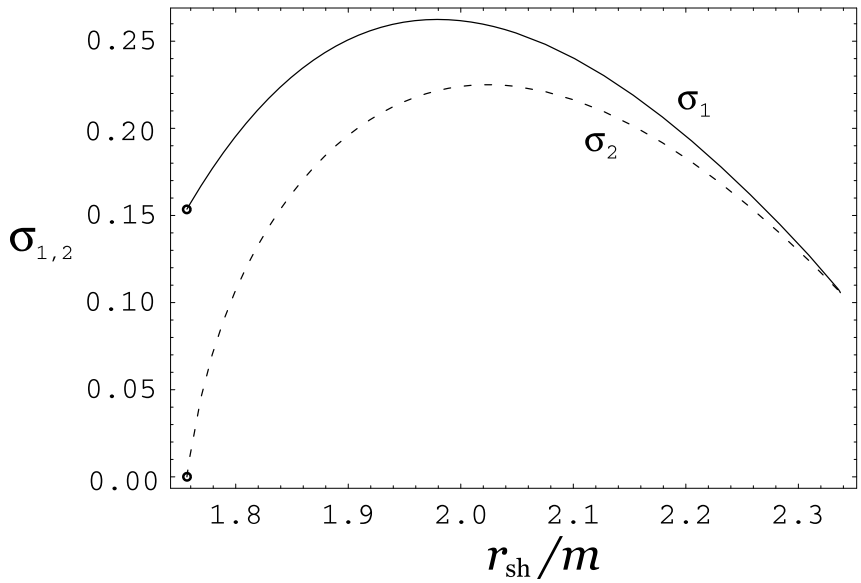

Fig. 8.— The upstream (solid curve) and downstream (dashed curve) magnetization parameters, σ_1 and σ_2, as a function of the shock location, for $a = 0.7m$ (see Table 2 for chosen flow parameters).

Conserved Parameter	Physical description	Definition
Ω_F	the angular velocity of the magnetic field lines	Eq.(8)
E	the total energy seen by a distant observer	Eq.(17)
L	the total angular momentum seen by a distant observer	Eq.(18)
η	the particle number flux per magnetic flux tube	Eq.(19)

Table 1: The table of conserved flow parameters. The mathematical definitions are expressed in the text (see, Bekenstein & Oron (1978); Camenzind (1986a)).

a/m	L/μ_1	$m\Omega_F$	$r_{\rm H}/m$	$r_{\rm L}/m$	$r_{\rm A}/m$	$r_{\rm inj}/m$	$r_{\rm sp}/m$
0.95	2.470	0.3691	1.312	1.314	1.335	1.439	1.457
0.70	3.137	0.2214	1.714	1.718	1.757	2.337	2.442
0.30	3.950	0.1096	1.954	1.964	2.022	3.694	4.270
0.00	5.073	0.0516	2.000	2.022	2.093	5.508	7.256
−0.20	7.332	0.0278	1.980	2.029	2.102	6.197	8.504
−0.40	10.233	0.0062	1.916	2.010	2.090	21.406	29.609

Table 2: The parameter sets for cold trans-fast MHD accretion solutions, where $E/\mu_1 = 1.006$, $\mu_1\eta = 0.041$ and $\mu_1 = m_{\rm p}$ (for a cold flow).

a/m	E/μ_1	L/μ_1	$m\Omega_F$	$\mu_1\eta$	$r_{\rm L}/m$	$r_{\rm A}/m$	$r_{\rm inj}/m$
0.0	1.00024	15.000	0.0019	0.0005	2.00003	2.001	44.6

Table 3: The parameter sets for cold trans-fast MHD accretion solutions.